

## Failure of Bohr's compound nucleus hypothesis for the $^{98}\text{Mo}(n,\gamma)^{99}\text{Mo}$ reaction\*

R. E. Chrien and G. W. Cole†

*Brookhaven National Laboratory, Upton, New York 11973*

G. G. Slaughter and J. A. Harvey

*Oak Ridge National Laboratory, Oak Ridge, Tennessee 37830*

(Received 8 September 1975)

Some remarkable features in the radiative deexcitation of narrow resonant states formed by slow neutron capture in  $^{98}\text{Mo}$  are pointed out. Earlier investigations indicating strong correlations between radiative widths and the single particle widths of both initial and final states involved in the reaction have been extended. A more precise set of resonance neutron widths has been developed from new total cross section measurements on isotopically separated molybdenum. From high resolution Ge(Li) detector measurements, a more complete set of  $\gamma$ -ray transition intensities was derived. The resulting intensities are compared with intensities calculated from the valence neutron transition model of Lynn, with dipole matrix elements calculated from the ABACUS code of Auerbach. We conclude that the valence model works surprisingly well for ground state transitions from resonances with reduced widths of larger than about  $10^{-3}$  single particle units. For smaller resonances, correlations persist, but these must be accounted for by other mechanisms.

[ NUCLEAR REACTIONS Partial radiative widths,  $^{98}\text{Mo}(n,\gamma)$ , neutron widths, spins, parities, valence model calculations, width correlations. ]

### I. INTRODUCTION

For some years it has been generally recognized that the narrow resonant states formed by slow neutron capture do not necessarily decay in the manner expressed by Bohr's compound nucleus hypothesis. Specifically, the partial widths for neutron absorption and decay show correlations, violating the assumption of independence for the formation and decay of the compound nuclear states. Such violations occur for both on-resonance and off-resonance capture; in the latter case there is a long history of correlations between thermal neutron capture  $\gamma$ -ray intensities and  $(d,p)$  cross sections. Lane and Lynn have developed a set of theories incorporating direct reaction mechanisms for both resonance and non-resonant radiative capture situations.<sup>1,2</sup> The theories are developed from a first-order perturbation approach incorporating photon widths into  $R$ -matrix theory according to the prescription of Lane and Thomas.<sup>3</sup> The theories may be classified following the description of the initial scattering state in the  $R$ -matrix approach. Thus "hard sphere capture" corresponds to the hard sphere scattering amplitude, "potential" capture corresponds to the scattering amplitude  $R'$ , containing the distant level contribution implicit in the optical model; "channel capture" (Ref. 4) corresponds to that part of the resonant scattering amplitude arising from contributions outside the nuclear

radius; and finally "valence capture" corresponds to single particle transitions in a complex potential well.

Refinements incorporating more complicated configurations of the capturing state have also been suggested. Clement, Lane, and Rook<sup>5</sup> included the coupling of the  $E1$  giant resonance to the single particle entrance channel in the "semi-direct" capture theories. This mechanism, as modified by Potokar,<sup>6</sup> has been reasonably successful in describing the capture of fast neutrons. Finally, Beer,<sup>7</sup> and Bartholomew and his co-workers<sup>8</sup> have pointed out the influence of three quasi-particle states on radiative decay to single particle final states. More recently, Soloviev and his colleagues<sup>9</sup> have attempted to describe "doorway states" in terms of a vibrational-single particle coupling model, while Beres and co-workers<sup>9</sup> have developed a description of doorways with an optical model potential.

These approaches have been partially, but not completely, successful in accounting for various aspects of neutron radiative capture. Recently,<sup>10</sup> it has been clearly established that potential capture is a good description for nonresonant (thermal neutron) capture near the region of the  $3s$  single particle resonance for slow neutrons ( $A \approx 40$ ), where the residual nuclei have low-lying  $2p$  states.

In resonance capture, correlations have been reported in mass regions corresponding to the  $3p$

TABLE I. Isotopic composition of Mo sample.

Isotope	92	94	95	96	97	98	100
% abundance	0.24	0.18	0.38	0.51	0.63	97.63	0.44

and 4s single particle resonances ( $A \approx 90$  and 150, respectively).<sup>11,12</sup> In the latter case the effect is marginal in terms of statistical significance. However, in the case of  $p$ -wave capture in the  $A \approx 90$  mass region, correlations of radiative transition strength with both initial and final state single particle widths are well established.

Several recent reviews are available which summarize in a comprehensive manner the non-statistical effects seen in neutron capture.<sup>13-16</sup>

In the present experiment, we have attempted to verify and extend the measurements on the radiative widths of the reaction  $^{98}\text{Mo}(n, \gamma)^{99}\text{Mo}$ . This reaction was previously studied for a limited set of resonances by the BNL fast chopper group,<sup>11</sup> who reported evidence for highly significant correlations between radiative widths and both neutron widths and final state ( $d, p$ ) spectroscopic factors. Subsequent measurements by Wasson and Slaughter,<sup>17</sup> Toohey and Jackson,<sup>18</sup> and Rimawi and Chrien<sup>19,20</sup> have confirmed the general presence of correlations in this mass region. Mughabghab *et al.*<sup>11</sup> were the first to point out the remarkable ability of the valence transition model to account qualitatively for these correlations. However, the number of resonances available to the chopper experiment was limited by the neutron energy resolution of that instrument; furthermore, the neutron widths for many of the resonances were not accurately determined. It seemed important therefore to extend these capture  $\gamma$ -ray measurements to beyond 1 keV and also to make further total cross section measurements in the keV region to establish accurate neutron widths and parity assignments. In order to do this we have taken advantage of the superior time-of-flight resolution available at the electron linear accelerator neutron source, ORELA, situated at Oak Ridge National Laboratory. A partial set of preliminary radiative widths for this experiment was previously reported by one of the authors (REC), at the Albany Conference on Statistical Properties of Nuclei, 1971.

## II. DESCRIPTION OF EXPERIMENT

This experiment is divided into two parts: a measurement of the partial radiative widths of  $^{98}\text{Mo}$  resonances to 5 keV using the 10-m capture  $\gamma$ -ray station at ORELA, and total cross section

measurements on two thicknesses of enriched  $^{98}\text{Mo}$  to about 50 keV using the 80-m flight path. Except for the reduction of total cross section data to transmissions and cross sections, including background corrections, all of the subsequent data analysis was performed at BNL. A description of the experimental details follows.

### A. Neutron total cross section of $^{98}\text{Mo}$

Total cross sections were measured on two thicknesses of 97.63% enriched  $^{98}\text{Mo}$ , 0.004 28 and 0.043 45 atom/b, in powdered oxide ( $\text{MoO}_3$ ) form. The measurements were made using a 1.27-cm thick  $^6\text{Li}$  glass scintillator at a flight path of 78.203 m and a nominal neutron burst width of 20 ns. Table I lists the isotopic composition of the sample. Transmission data were obtained by cycling the  $^{98}\text{Mo}$  sample, background samples, and a blank holder. Time-of-flight dependent backgrounds were determined by the techniques of inserting samples of polythene and samples of uranium, copper, and iron with "blacked-out" resonances, that is resonances whose expected minimum transmissions were sufficiently close to zero over the time region of interest. At short flight times, the background is almost completely due to 2.23-MeV  $\gamma$  rays from neutron capture in the water moderator around Ta target. This neutron source decays with a  $\sim 17$ - $\mu\text{s}$  decay time after the burst. The polythene scatters virtually all neutrons from the beam and permits one to measure this  $\gamma$ -ray background. The molybdenum samples were collimated to a diameter of 2.74 cm perpendicular to the 2.38-cm diam neutron beam. All runs were made with a beam filter of 0.635 cm of lead and 0.6 g/cm<sup>2</sup> of  $^{10}\text{B}$  to eliminate low-energy  $\gamma$  rays and overlap neutrons in the beam.

The data were reduced to transmission form with appropriate background corrections and error calculations by use of the standard ORELA code called "4TJACK." The data were sorted into time channels of widths appropriate to the resolution available in the time region. The ORELA data were converted to a format suitable for the CDC 6600 system at BNL. Transmission dip area data were then analyzed by a BNL version of the Atta-Harvey code called "FASCHOP,"<sup>22</sup> and a set of resonance parameters produced. A comparison of thin and thick sample data was performed in order to produce a consistent set of neutron widths,  $g\Gamma_n$ .

For the conclusions of the present experiment, the  $l$ -value assignments of the resonances, particularly the very large  $p$ -wave resonances at 429, 612, and 817 eV, are crucial. Because of this fact, we discuss our assignment in some detail. It is possible to assign  $l$  values for resonances in one of the following ways:

(1) From measurements of the neutron width and applying a Bayes' theorem type calculation based on the size of the neutron widths. This probabilistic argument works best at low energies. It becomes suspect in the cases where anomalously large  $p$ -wave widths may be present, since it is just those cases which we must be careful to distinguish from  $l=0$  resonances.

(2) From measurements of the shape asymmetry of resonance transmission dips. The shape asymmetry is a characteristic of interference between resonance and potential scattering.

(3) From angular correlation measurements in resonance scattering or  $\gamma$ -ray emission. The resonance shape may indicate the resonance-potential interference, for  $J > \frac{1}{2}$ , may indicate the resonance angular momentum. This latter effect was used in our earlier<sup>11</sup> work to assign a  $p$ - $\frac{3}{2}$  character to the 817-eV resonance.

In the present study we apply methods (1) and (2). As an example, we show the measured and fitted transmissions in the vicinity of the 429-eV resonance in Fig. 1. No asymmetry is apparent; the calculated asymmetry expected on the basis of an  $l=0$  assignment for this resonance is also shown. Our experiment allows us to conclude with confidence that the 429 resonance is a  $p$ -wave reso-

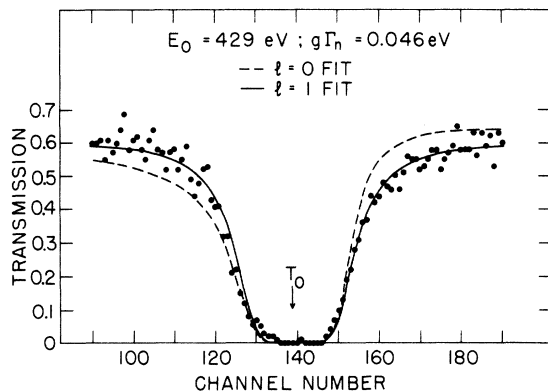


FIG. 1. Time-of-flight plot of the thick sample transmission data near 429-eV resonance. The channel width is 32 ns and the instrumental resolution is approximately two channels full width at half maximum. Shown are fits for  $l=1$  (—) and  $l=0$  (---) assignments which give the same area. The latter is ruled out by the symmetric shape observed.

nance, since higher  $l$  values are excluded because of their small penetrabilities. Similar conclusions led to the other assignments of the present work. We do not assign parities beyond 10 keV because of the resolution problem coupled with increasing  $p$ -wave penetrabilities, which make a clean separation more difficult.

The present assignments for the important  $p$ -wave resonances at 429, 611, and 817 eV are supported by the neutron scattering experiments of Migneco, Theobald, and DeJonge.<sup>23</sup> Furthermore, although  $l$  values are not reported, the Columbia data of Wynchank *et al.*<sup>24</sup> show no  $s$ -wave asymmetries for these important data. The parity assignments adopted by BNL-325 (Ref. 25) are based on unpublished data of Newstead.<sup>26</sup> Our data are in agreement with this evaluation. However, the earlier transmission work of Shwé and Coté<sup>27</sup> report the observation of asymmetries for the 429-, 612-, and 817-eV resonances. We do not believe their claim is supportable for the following reasons:

(a) The time-of-flight resolution of 11 ns/m of their experiment is about a factor of 50 worse than that of the present experiment. We think it unlikely that the asymmetry expected for  $s$ -wave assignments could be seen at that resolution level.

(b) No samples enriched in <sup>98</sup>Mo were used previously. In view of the natural abundance of <sup>98</sup>Mo, 24.4%, the purported asymmetries would be reduced by about a factor of 4.

(c) The thickest sample used by Shwé and Coté was thinner by 25% than that of the present experiment.

In view of these factors, and our nonobservation of these crucial asymmetries, we can only conclude that the asymmetries reported by Shwé and Coté were instrumental effects.

The probabilistic approach to the assignment of resonance  $l$  values is based on the application of Bayes' theorem, as first suggested for this application by Bollinger and Thomas.<sup>28</sup> From the theorem, and the properties of the Porter-Thomas distribution, it is possible to write the probability of a level with a measured  $g\Gamma_n$  having  $l=1$ , when only  $l=0$  and  $l=1$  are considered:

$$P(l=1) = \left\{ 1 + \frac{1}{3} (S_1/S_0)^{1/2} P_1^{1/2} \exp[(g\Gamma_n/2\sqrt{E_0}\langle D_0 \rangle) \times (1/P_1 S_1 - 1/S_0)] \right\}^{-1} \quad (\text{for target spin zero}),$$

when  $P_1$  is the  $p$ -wave penetrability,  $k^2 R^2 / (1 + k^2 R^2)$  and  $S_0, S_1$  are the  $s$ - and  $p$ -wave strength functions, and  $\langle D_0 \rangle$  is the  $l=0$  resonance spacing.

We calculated  $P(l=1)$ , given the strength functions listed in BNL-325,<sup>25</sup> and the level spacing  $D_0 = 900$  eV, deduced from the listed  $l=0$  resonances below 5 keV, in that evaluation. The re-

TABLE II. *s*-wave neutron reduced widths for  $^{98}\text{Mo}$ .

$E_0$ (eV)	$\Gamma_n^0$ (meV)
467.0 ± 0.3	35.1 ± 2.0
1525.0 ± 1.0	32.8 ± 3.0
2546.3 ± 1.5	17.6 ± 3.0
3293.0 ± 1.9	25.8 ± 3.0
4475.0 ± 2.6	6.4 ± 1.0
5596.0 ± 3.7	26.0 ± 2.0
6178.0 ± 3.7	84.0 ± 10.0
7497.0 ± 4.4	46.6 ± 5.0
9032.0 ± 5.4	377.0 ± 50.0
10576.0 ± 6.0	117.0 ± 15.0

sults for the important resonances at 429, 612, and 817 eV are 0.59, 0.84, and 0.72, respectively. It appears that the Bayes's theorem test is not a useful one at energies above a few hundred eV because of the rapid increase in *p*-wave penetrabilities and consequent overlapping of *p*- and *s*-wave width distributions.

The sharp disagreements with  $P(l=1)$  estimates of Shwé and Coté are again notable. Those authors assign *P* values of  $10^{-4}$  or less for these resonances. They fail to point out, however, that a knowledge of  $\langle D_0 \rangle$  is required to calculate  $P(l=1)$ , and they do not indicate the value of  $\langle D_0 \rangle$  they assumed. We can only conclude that they used an unrealistic value of  $\langle D_0 \rangle$ . The  $P(l=1)$  values are extremely sensitive to  $\langle D_0 \rangle$ ; for the 429-eV level the value of *P* decreases by a factor of  $10^4$  for a factor of 4 decrease in  $\langle D_0 \rangle$ .

Although transmission data were analyzed to above 100 keV, we did not consider neutron energy resolution adequate to list resonance parameters above 50 keV. Up to 20 keV parameters were derived from both thick and thin sample data. Above 20 keV the listed parameters are derived from the thick sample data only. Since  $\Gamma_n > \Gamma_\gamma$  for most resonances, it is not sensible to try to obtain total radiation widths from these data. We used the  $\gamma$ -ray data for spin assignments of resonances relevant to this work (below about 5 keV for the detailed checks of the valence model). The results of these analyses are given in Tables II-IV. Tables II and III list the *s*- and *p*-wave reduced widths for the  $l=0$  and  $l=1$  resonances, respectively, as defined by the relations  $g\Gamma_n^0 = g\Gamma_n E_0^{-1/2}$  and  $g\Gamma_n^1 = g\Gamma_n E_0^{-1/2}[1 + (ka)^{-2}]$ , where *E* is expressed in eV and  $a = 6.62 \times 10^{-13}$  cm. Above 10 keV, in Table IV, only the parameter  $g\Gamma_n E^{-1/2}$  is listed, since we are not able to assign parities with confidence. The previously known resonance parameters and a list of references to measurements are given in BNL-325.<sup>25</sup>

TABLE III. *p*-wave neutron reduced widths for  $^{98}\text{Mo}$ .

$E_0$ (eV)	$g\Gamma_n^1$ (eV)
12.1 ± 0.15	0.75 ± 0.04
401.4 ± 0.3	0.179 ± 0.02
428.8 ± 0.3	3.99 ± 0.24
611.8 ± 0.4	2.10 ± 0.35
817.3 ± 0.5	2.81 ± 0.28
1121.9 ± 0.7	0.24 ± 0.05
1919.5 ± 1.2	0.075 ± 0.03
2175.8 ± 1.2	0.81 ± 0.14
2460.0 ± 1.5	0.370 ± 0.06
2610.0 ± 1.6	0.10 ± 0.02
2943.0 ± 1.8	0.072 ± 0.02
3260.0 ± 1.9	0.053 ± 0.04
3794.0 ± 2.3	0.775 ± 0.16
4013.0 ± 2.4	0.33 ± 0.05
4567.0 ± 2.7	0.52 ± 0.10
4844.0 ± 2.9	0.596 ± 0.10
5268.0 ± 3.2	1.49 ± 0.45
5636.0 ± 3.4	0.74 ± 0.12
5915.0 ± 3.5	1.247 ± 0.25
6675.0 ± 4.0	0.16 ± 0.08
6814.0 ± 4.1	0.769 ± 0.16
7172.0 ± 4.3	0.148 ± 0.08
7590.0 ± 4.6	0.377 ± 0.07
7960.0 ± 4.8	0.625 ± 0.12
8558.0 ± 5.2	1.56 ± 0.25
8815.0 ± 5.3	0.710 ± 0.17
9362.0 ± 5.6	0.114 ± 0.05
9659.0 ± 5.8	0.792 ± 0.16
9723.0 ± 5.9	0.110 ± 0.05
10025.0 ± 6.0	0.192 ± 0.05

### B. Partial radiative widths

Neutron capture  $\gamma$ -ray radiation from a 50-g sample of  $^{98}\text{Mo}$  was recorded with a 31.7-cm<sup>3</sup> Ge(Li) true coaxial detector at the 10-m flight path of ORELA. The detector (ORTEC Model 8001-0523 Serial 9-571) had a resolution of 6.9 keV full width at half maximum at 6 MeV and viewed the sample through shielding of 0.635 cm Pb and 5.08 cm of  $^6\text{Li}$ -loaded paraffin. Capture spectra from resonances were recorded in a multiparameter system based on a disk memory of the ORELA 810B computer system. In this arrangement 71 pulse height spectra of 4096 channels each, corresponding to preselected time-of-flight gates could be recorded on the disk. In addition single parameter time-of-flight and pulse height spectra were also recorded. Neutron burst widths of 6.5 to 40 ns were obtained from ORELA, with most of the data recorded at 20 ns.

Although spectra up to neutron energies of ~10 keV were obtained, only partial widths for resonances up to about 5 keV were extracted, since

TABLE IV. Neutron widths unassigned as to parity for  $^{98}\text{Mo}$ .

$E_0$ (eV)	$g \Gamma_n^0$ (meV)						
10 868 ± 6	6.5 ± 2.0	19 247 ± 14	33.0 ± 6.0	29 372 ± 21	11.0 ± 3.0	40 721 ± 31	20.0 ± 5.0
11 283 ± 6	3.0 ± 2.0	19 575 ± 14	67.0 ± 13.0	29 757 ± 21	9.0 ± 3.0	41 298 ± 32	25.0 ± 6.0
11 330 ± 6	29.0 ± 6.0	19 965 ± 14	6.0 ± 3.0			41 673 ± 32	32.0 ± 6.0
11 564 ± 6	18.0 ± 5.0	20 197 ± 14	9.0 ± 4.0	30 595 ± 22	251.0 ± 50.0	42 929 ± 33	54.0 ± 11.0
11 672 ± 6	64.0 ± 15.0			30 655 ± 22	47.0 ± 9.0	42 970 ± 33	11.0 ± 4.0
11 984 ± 7	52.0 ± 7.0	21 879 ± 15	21.0 ± 5.0	31 105 ± 22	20.0 ± 5.0	43 967 ± 33	11.0 ± 4.0
		22 003 ± 15	29.0 ± 6.0	31 437 ± 22	18.0 ± 5.0		
12 067 ± 7	10.4 ± 3.0	22 496 ± 15	11.0 ± 3.0	31 933 ± 23	29.0 ± 6.0	44 084 ± 33	16.0 ± 5.0
13 123 ± 8	7.1 ± 2.0	22 903 ± 16	11.0 ± 3.0	32 048 ± 23	36.0 ± 7.0	44 334 ± 33	51.0 ± 11.0
13 397 ± 8	18.0 ± 6.0	23 464 ± 16	76.0 ± 15.0			44 700 ± 33	72.0 ± 16.0
14 583 ± 9	4.5 ± 2.0	23 610 ± 16	7.0 ± 2.0	32 362 ± 23	22.0 ± 5.0	45 124 ± 34	287.0 ± 60.0
14 741 ± 9	42.0 ± 10.0			33 315 ± 24	28.0 ± 6.0	45 657 ± 34	130.0 ± 30.0
14 782 ± 9	31.0 ± 6.0	24 286 ± 17	12.0 ± 3.0	33 709 ± 24	17.0 ± 4.0	45 823 ± 35	15.0 ± 5.0
		24 490 ± 17	49.0 ± 10.0	33 877 ± 25	41.0 ± 9.0		
15 210 ± 10	12.4 ± 3.0	24 831 ± 17	6.0 ± 2.0	36 035 ± 26	114.0 ± 20.0	45 949 ± 35	72.0 ± 16.0
15 897 ± 10	11.9 ± 3.0	25 457 ± 18	36.0 ± 7.0	36 792 ± 26	70.0 ± 15.0	47 128 ± 36	18.0 ± 6.0
16 181 ± 11	6.0 ± 2.0	25 544 ± 18	10.0 ± 3.0			48 428 ± 37	131.0 ± 27.0
16 455 ± 11	19.0 ± 5.0	26 851 ± 19	6.0 ± 3.0	37 068 ± 27	18.0 ± 5.0	49 144 ± 38	14.0 ± 7.0
16 684 ± 12	6.0 ± 2.0			37 635 ± 27	88.0 ± 18.0	49 265 ± 38	41.0 ± 13.0
16 945 ± 12	25.0 ± 5.0	27 056 ± 19	31.0 ± 6.0	38 217 ± 28	162.0 ± 35.0	49 786 ± 39	91.0 ± 30.0
		27 588 ± 19	7.0 ± 3.0	38 668 ± 29	115.0 ± 22.0	52 071 ± 40	40.0 ± 20.0
17 594 ± 13	27.5 ± 5.0	27 771 ± 20	18.0 ± 4.0	39 455 ± 30	28.0 ± 6.0	52 600 ± 40	96.0 ± 30.0
18 284 ± 13	7.0 ± 2.0	28 614 ± 20	60.0 ± 10.0	39 967 ± 30	19.0 ± 5.0		

limitations on useful flux and higher backgrounds in the 5–10-keV region prevented meaningful analysis.

The  $\gamma$ -ray energy scale was fixed using the known energies of background lines in the spectra. These included the hydrogen capture line at 2223.9 keV, ThC'' at 2614.47 keV,  $^{56}\text{Fe}$  capture lines at 5920.9, 6018.4, 7279.1, 7631.5, and 7645.6 keV, and the  $m_e c^2$  energy differences between full energy, single, and double escape peaks from the detector. Spectra were recorded at a gain of 2.430 keV/channel, from about 500 to 9900 keV. The neutron separation energy for  $^{99}\text{Mo}$  was determined to be  $5924.6 \pm 0.6$  keV after correction for nuclear recoil. The corresponding energy for the ground state transition is 5924.4 keV. The previously accepted values are  $5924 \pm 3$  keV (Ref. 25) and  $5917 \pm 6$  from the Wapstra-Gove mass tables.<sup>31</sup> Seventeen  $p$ -wave and five  $s$ -wave resonances in the interval 0–5268 eV had sufficient intensities in their  $\gamma$  spectra to permit data reduction with a least-squares area analysis based on a Gaussian fit to the known resolution function of the detector. Figure 2 gives the time-of-flight plot in this region for events exceeding 500 keV deposited in the detector.

For absolute calibration of photon intensities, the ORELA data were normalized to the earlier BNL data up to 1 keV. The latter were in turn referred to the absolute intensities for  $^{197}\text{Au}(n, \gamma)$ - $^{198}\text{Au}$  due to Kane, at the resonance near 4.9 eV.<sup>32</sup>

(These are essentially equivalent to the reported results of Loper, Thomas, and Bollinger.<sup>33</sup>) For the purposes of converting recorded intensities to partial widths or vice versa, the angular correlations for  $p_{3/2} \rightarrow s_{1/2}$ ,  $d_{3/2}$ ,  $d_{5/2}$  were taken into account. In the tables of experimental results which follow, the data represent photons/capture recorded at  $90^\circ$  to the beam, and the calculations of the valence model, when converted to intensities, include the angular correlation factors.

The reduction of peak areas to absolute photon intensities follows normally accepted procedure. The total counting rate in the interval 500–6000 keV is assumed proportional to the total capture rate, after suitable background is subtracted. This background was determined from off-resonance scan regions. In the region of interest in this experiment, 5–6 MeV, the variation in detector efficiency in the two-escape mode is relatively small and did not contribute significantly to the error in photon intensity assignments. For levels populated in  $^{99}\text{Mo}$  up to an excitation energy of about 1 MeV, we give intensity data; these are compared with the predictions of the valence model. A complete list of the  $\gamma$  rays observed in  $^{98}\text{Mo}(n, \gamma)^{99}\text{Mo}$ , the levels populated in  $^{99}\text{Mo}$ , and the deduced spin-parity are given in Table V. The resonance intensities for transitions to levels below 1 MeV excitation are given in Table VI ( $s$  wave) and Table VII ( $p$  wave).

In general intensities are derived from two-

escape peak areas, and corrected, where necessary, by the overlap of full energy and one-escape peaks on the two-escape peak of interest. For the detector used the ratios of full energy and one-escape peak to two-escape peak areas were  $0.51 \pm 0.03$  and  $0.36 \pm 0.03$ , respectively, in the range 5–6 MeV.

Resonance widths for transitions to states above 1 MeV in excitation were calculated, but are not included in tabular form. They are available on request in the files of the National Neutron Cross Section Center, Brookhaven National Laboratory.

Perhaps the most arresting feature apparent from viewing the spectra is the relative dominance of the ground state transitions in many of the  $p$ -wave resonances. The absolute strengths of the other transitions are not unusual, however. If we

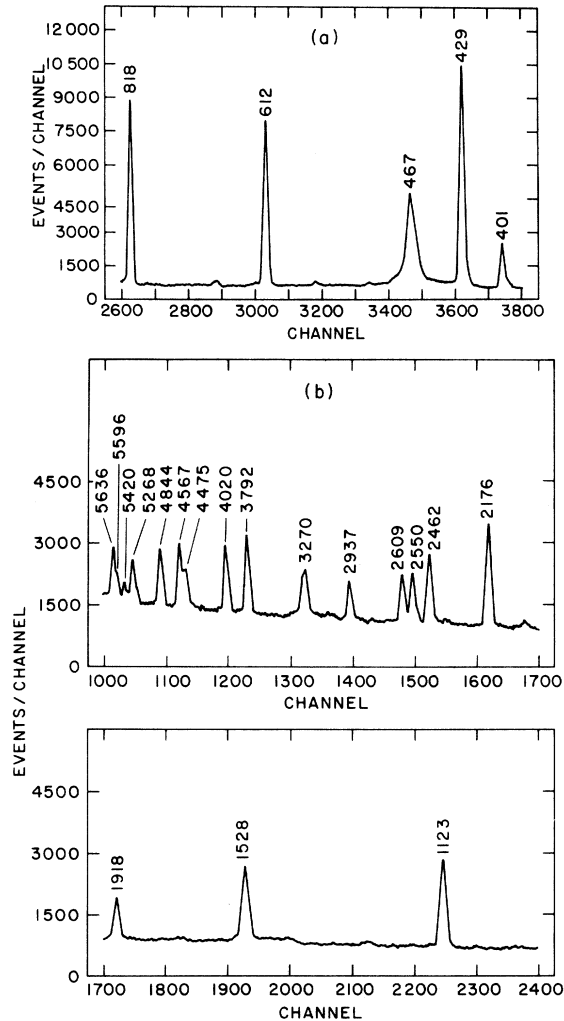


FIG. 2. (a) Time-of-flight plot of events in the Ge(Li) detector for the energy region from 401 to 900 eV, and (b) 1 to 5.6 keV.

TABLE V. Capture  $\gamma$ -ray line list for  $^{98}\text{Mo}(n, \gamma)^{99}\text{Mo}$ .

$E_\gamma$ (keV)	$E_{\text{exc}}$ (keV)	$J^\pi$	$l$
$5924.4 \pm 0.6$	0.0	$\frac{1}{2}^+$	0
$5827.0 \pm 1.2$	97.35	$\frac{5}{2}^+$	2
$5573.1 \pm 0.8$	351.3	$\frac{3}{2}^+$	2
$5399.8 \pm 1.0$	524.6	$\frac{1}{2}^+$	0
$5375.8 \pm 0.8$	548.6	$\frac{3}{2}^+$	2
$5310.6 \pm 1.2$	613.8	$\frac{5}{2}^+$	2
$5293.1 \pm 1.2$	631.3	$(\frac{5}{2})^+$	
$5132.6 \pm 0.8$	791.8	$\frac{3}{2}^+$	2
$5037.0 \pm 1.0$	887.4	$\frac{3}{2}^+$	2
$5019.4 \pm 0.8$	905.0	$\frac{1}{2}^+$	0
$4979.4 \pm 1.2$	945.0		
$4899.6 \pm 0.8$	1024.8	$\frac{1}{2}^-, \frac{3}{2}^-$	1
$4758.2 \pm 0.8$	1166.2	(+)	
$4670.7 \pm 1.0$	1253.7	(+)	
$4542.6 \pm 1.2$	1381.8	$\frac{3}{2}^+, \frac{5}{2}^+$	2
$4469.2 \pm 2.0$	1455.2		
$4391.4 \pm 2.0$	1533.0		
$4365.4 \pm 1.2$	1559.0		
$4353.5 \pm 1.2$	1570.9		
$4289.7 \pm 2.0$	1634.7	(+)	
$4263.4 \pm 2.4$	1661.0		
$4214.3 \pm 1.8$	1710.0	$\frac{1}{2}^-, \frac{3}{2}^-$	1
$4183.0 \pm 2.0$	1741.0	$\frac{3}{2}^-, \frac{5}{2}^-$	2
$4037.0 \pm 2.4$	1888.0		
$3996.0 \pm 2.0$	1928.0	(-)	
$3975.0 \pm 2.0$	1950.0		
$3869.0 \pm 2.0$	2055.0	(+)	
$3792.0 \pm 2.0$	2132.0		
$3745.0 \pm 2.4$	2179.0		
$3706.0 \pm 2.4$	2218.0		
$3625.0 \pm 2.4$	2299.0		
$3606.0 \pm 2.0$	2318.0		
$3584.0 \pm 2.0$	2341.0		

compute the photon strength function for  $^{99}\text{Mo}$ , from the relations

$$k_{E1} = (\langle \Gamma_{\gamma\lambda f} \rangle / D) A^{-2/3} E_\gamma^{-3} \text{ (MeV}^{-3}\text{)},$$

$$k_{M1} = (\langle \Gamma_{\gamma\lambda f} \rangle / D) E_\gamma^{-3} \text{ (MeV}^{-3}\text{)},$$

we obtain the values  $k_{E1} = 1.8 \times 10^{-9}$  and  $k_{M1} = 4.9 \times 10^{-9}$ . These values are obtained after a

TABLE VI. *s*-wave resonance  $\gamma$ -ray intensities. Intensities are listed in photons/capture.

$E_\gamma$ (keV)	$E_x$ (keV)	$J^\pi$	$E_0$ (eV)				
			467 $\frac{1}{2}^+$	1525 $\frac{1}{2}^+$	2546 $\frac{1}{2}^+$	3293 $\frac{1}{2}^+$	4475 $\frac{1}{2}^+$
5924.4	0	$\frac{1}{2}^+$	<0.005	0.013 $\pm$ 0.010	<0.010	0.012 $\pm$ 0.006	0.009 $\pm$ 0.005
5827.0	97	$\frac{5}{2}^+$	<0.005	<0.010	<0.010	<0.012	<0.020
5573.1	351	$\frac{3}{2}^+$	0.030 $\pm$ 0.002	0.015 $\pm$ 0.010	<0.010	<0.012	0.019 $\pm$ 0.010
5399.8	525	$\frac{1}{2}^+$	<0.005	0.030 $\pm$ 0.006	<0.010	0.010 $\pm$ 0.003	<0.020
5375.8	549	$\frac{3}{2}^+$	0.020 $\pm$ 0.005	<0.010	<0.010	0.011 $\pm$ 0.004	<0.020
5310.6	614	$\frac{5}{2}^+$	<0.005	<0.010	<0.010	<0.012	<0.020
5293.1	631	$\frac{3}{2}^+$	<0.005	<0.010	0.008 $\pm$ 0.004	<0.012	0.014 $\pm$ 0.007
5132.6	792	$\frac{3}{2}^+$	0.013 $\pm$ 0.005	0.011 $\pm$ 0.006	<0.010	<0.012	0.011 $\pm$ 0.006
5037.4	887	$\frac{3}{2}^+$	<0.005	0.007 $\pm$ 0.002	0.006 $\pm$ 0.002	<0.012	<0.020
5019.4	905	$\frac{1}{2}^+$	<0.005	0.024 $\pm$ 0.008	0.016 $\pm$ 0.012	0.012 $\pm$ 0.002	<0.020

correction for transition strengths below experimental sensitivity, based on the Porter-Thomas distribution. They are near the values of 3 and  $4 \times 10^{-9}$  typical for medium to heavy nuclides at the neutron binding energy.<sup>34</sup> The ratio of  $\Gamma(E1)/\Gamma(M1)$  is 6.1, as compared with the 7 estimated by Bollinger.<sup>14</sup>

Typical pulse height spectra for this experiment are shown in Fig. 3. The figure shows the spectrum for the 12-eV resonance, which possesses an average sized neutron width, and the 612-eV spectrum, which is characteristic of a resonance with an exceedingly large neutron width. For comparison the spectrum of an *s*-wave resonance,  $E_0 = 467$  eV, is also shown.

### III. RESULTS AND DISCUSSION

#### A. Nuclear structure of $^{99}\text{Mo}$

The low-lying levels of  $^{99}\text{Mo}$  have been mapped out previously by radioactive decay<sup>35</sup> of 2.6-min  $^{99}\text{Nb}$ , by (*d, p*),<sup>36</sup> (*d, t*),<sup>37</sup> and by (*p, d*) (Ref. 38) reaction data. The diagram of Fig. 4 serves to summarize previously known levels to 2.3 MeV and to indicate schematically the information provided in the present experiment. The previous work has been evaluated by Medsker.<sup>39</sup>

To a crude approximation the low-lying levels of  $^{99}\text{Mo}$  can be understood by considering the  $N = 50$  major neutron shell closure at  $^{92}\text{Mo}$  and the minor  $d_{5/2}$  shell closure at  $^{98}\text{Mo}$ . The low-lying levels of  $^{99}\text{Mo}$  have largely *s*- and *d*-wave character, as has been established from the (*d, p*) experiments. The ground state of  $^{99}\text{Mo}$  is a relatively pure single particle  $s_{1/2}$  state, as is evidenced by the (*d, p*) spectroscopic factor of 0.67.

Thus  $^{98}\text{Mo}(n, \gamma)^{99}\text{Mo}$  is expected to be a good candidate for direct transitions from the capture state which bypass compound nucleus formation.

In the following paragraphs of this section we make some specific comments on the results of the present experiment (Table V) of relevance to the level structure of  $^{99}\text{Mo}$ . We note that many of the levels strongly populated in the (*d, p*) reaction are also seen in resonance (*n, \gamma*) work and need no comment. In particular, the ground state transition is strongly observed in most *p*-wave resonances and is seen also as an *M1* transition in the *s*-wave resonances. The levels seen here agree well in energy with the (*d, p*) levels of Ref. 36 below 0.5 MeV excitation; however, there is an increasing discrepancy above that energy, reaching 12 keV at 1700 keV. A similar discrepancy is apparent in comparing the results of other experiments with (*d, p*); hence, we attribute the discrepancy to an error in the energy scale for the (*d, p*) reaction experiments.

Comments on specific levels follow. The  $\gamma$ -ray energy is listed, followed by the excitation energy,  $l$  value, and spin-parity of the final state. Transitions labeled \* lead to states not previously observed.

5924 (ground state;  $l = 0; \frac{1}{2}^+$ ). A relatively strong line in most  $\frac{1}{2}^-$ ,  $\frac{3}{2}^-$  resonances.

5827 (97 keV;  $l = 2; \frac{5}{2}^+$ ). This level is not populated in any of the six  $\frac{1}{2}^-$  resonances, or the five  $\frac{1}{2}^+$  resonances, so the  $\frac{5}{2}^+$  assignment is indicated.

5573.1 (351 keV;  $l = 2; \frac{3}{2}^+$ ). This level is populated by resonances with  $\frac{1}{2}^+$ , hence,  $\frac{3}{2}^+$  is required.

5400 (524 keV;  $l = 0; \frac{1}{2}^+$ ).

5376 (548 keV;  $l = 2; \frac{3}{2}^+$ ). The  $\frac{3}{2}^+$  assignment is mandated by observation of the  $\gamma$  ray from  $\frac{1}{2}^-$

TABLE VII.  $p$ -wave resonance  $\gamma$ -ray intensities. Intensities in photons/capture observed at  $90^\circ$  to the beam. Listed in parentheses below the observed intensities are the model predictions, evaluated at  $90^\circ$ . < means unobserved, and less than indicated upper limit. (<) means less than 0.0001 calculated.

$E_\gamma$ (keV)	$E_x$ (keV)	$J^\pi$	$E_0$ (eV)							
			12.1 $\frac{3}{2}^-$	401 $\frac{3}{2}^-$	428.8 $\frac{1}{2}^-$	611.8 $\frac{1}{2}^-$	817.3 $\frac{3}{2}^-$	1121.9 $\frac{3}{2}^-$	1919.5 $\frac{3}{2}^-$	2175.8 $\frac{1}{2}^-$
5924.4	0	$\frac{1}{2}^+$	0.0285 ± 0.001 (0.0952)	0.0189 ± 0.0038 (0.0249)	0.203 ± 0.009 (0.313)	0.190 ± 0.006 (0.226)	0.107 ± 0.003 (0.276)	0.020 ± 0.003 (0.0329)	< 0.010 (0.0112)	0.027 ± 0.004 (0.118)
5827.0	97	$\frac{3}{2}^+$	0.0045 ± 0.0011 (0.0192)	0.050 ± 0.001 (0.00526)	...	...	< 0.003 (0.0553)	< 0.005 (0.00576)	< 0.010 (0.00236)	...
5573.1	351	$\frac{3}{2}^+$	0.0158 ± 0.002 (0.000812)	0.016 ± 0.008 (0.000812)	0.141 ± 0.007 (0.0435)	0.122 ± 0.005 (0.0315)	0.021 ± 0.010 (0.00251)	0.012 ± 0.006 (0.000878)	0.008 ± 0.004 (0.000830)	< 0.008 (0.00182)
5399.8	525	$\frac{1}{2}^+$	< 0.002 (0.00508)	< 0.005 (0.00138)	0.020 ± 0.001 (0.0147)	0.013 ± 0.008 (0.0107)	0.005 ± 0.002 (0.0137)	< 0.008 (0.00137)	< 0.008 (0.000830)	0.015 ± 0.002 (0.00546)
5375.8	549	$\frac{3}{2}^+$	0.032 ± 0.001 (0.00325)	< 0.005 (0.000884)	0.094 ± 0.005 (0.152)	0.059 ± 0.008 (0.110)	0.009 ± 0.001 (0.00880)	< 0.008 (0.000878)	< 0.010 (0.000830)	0.016 ± 0.002 (0.0573)
5310.6	614	$\frac{5}{2}^+$	< 0.002 (0.00107)	0.008 ± 0.002 (0.00107)	...	...	< 0.005 (0.00412)	0.022 ± 0.003 (0.000878)	0.020 ± 0.003 (0.000830)	...
5293.1	631	$\frac{3}{2}^+$	< 0.002 (0.00107)	0.019 ± 0.001 (0.00107)	< 0.002 (0.00107)	< 0.008 (0.00107)	< 0.005 (0.00412)	0.005 ± 0.005 (0.000878)	0.0074 ± 0.004 (0.000830)	0.044 ± 0.005 (0.000830)
5132.6	792	$\frac{3}{2}^+$	0.057 ± 0.002 (0.00132)	0.0096 ± 0.004 (0.00132)	< 0.002 (0.0132)	0.0078 ± 0.002 (0.00938)	0.012 ± 0.002 (0.000628)	0.022 ± 0.004 (0.000628)	0.038 ± 0.019 (0.000628)	0.029 ± 0.002 (0.00455)
5037.4	887	$\frac{3}{2}^+$	0.013 ± 0.001 (0.000812)	< 0.005 (0.000812)	< 0.005 (0.0269)	< 0.008 (0.0194)	0.008 ± 0.002 (0.00126)	0.023 ± 0.002 (0.00126)	0.007 ± 0.002 (0.00126)	< 0.010 (0.0100)
5019.4	905	$\frac{1}{2}^+$	0.062 ± 0.003 (0.00127)	0.005 ± 0.003 (0.00127)	0.0035 ± 0.0005 (0.00587)	0.011 ± 0.004 (0.00402)	0.005 ± 0.0005 (0.00491)	0.0065 ± 0.003 (0.00491)	0.0093 ± 0.001 (0.00491)	< 0.008 (0.00182)
$E_\gamma$ (keV)	2460	$\frac{1}{2}^-$	2610	2943	3260	3794	4013	4567	4844	5268
5924.4	0.011 ± 0.005 (0.0598)	$\frac{1}{2}^-$	0.020 ± 0.010 (0.0140)	0.044 ± 0.011 (0.0122)	0.029 ± 0.005 (0.00895)	0.089 ± 0.010 (0.0987)	0.006 ± 0.003 (0.0458)	0.102 ± 0.010 (0.0683)	0.023 ± 0.010 (0.0778)	< 0.015 (0.171)
5827.0	...	$\frac{3}{2}^-$	< 0.008 (0.00235)	...	...	< 0.010 (0.0191)	0.080 ± 0.016 (0.00906)	0.006 ± 0.003 (0.0144)	0.033 ± 0.017 (0.0152)	0.021 ± 0.011 (0.0347)
5573.1	0.022 ± 0.011 (0.00811)	$\frac{3}{2}^-$	< 0.008 (0.000811)	0.018 ± 0.009 (0.00222)	< 0.008 (0.00112)	< 0.010 (0.000810)	0.008 ± 0.002 (0.000810)	0.008 ± 0.002 (0.000810)	< 0.012 (0.000830)	0.016 ± 0.008 (0.00147)
5399.8	< 0.008 (0.00304)	$\frac{3}{2}^-$	< 0.008 (0.000811)	0.019 ± 0.010 (0.00111)	0.012 ± 0.006 (0.00447)	< 0.010 (0.00506)	< 0.010 (0.00173)	< 0.012 (0.00168)	< 0.012 (0.00249)	< 0.015 (0.00587)
5375.8	< 0.008 (0.0294)	$\frac{3}{2}^-$	0.034 ± 0.010 (0.00666)	< 0.008 (0.00666)	< 0.008 (0.00447)	0.009 ± 0.004 (0.00324)	< 0.010 (0.00106)	< 0.012 (0.00110)	< 0.012 (0.00109)	< 0.015 (0.00289)
5310.6	...	$\frac{3}{2}^-$	< 0.008 (0.000811)	...	...	< 0.010 (0.00106)	< 0.010 (0.00106)	< 0.012 (0.00110)	< 0.012 (0.00109)	< 0.015 (0.00289)
5293.1	0.011 ± 0.006 (0.00107)	$\frac{3}{2}^-$	0.011 ± 0.004 (0.00107)	< 0.008 (0.00107)	0.014 ± 0.007 (0.00107)	< 0.010 (0.00106)	0.012 ± 0.006 (0.00110)	0.011 ± 0.002 (0.00110)	0.012 ± 0.006 (0.00109)	< 0.015 (0.00289)
5132.6	< 0.008 (0.00203)	$\frac{3}{2}^-$	0.013 ± 0.006 (0.00203)	0.006 ± 0.004 (0.00203)	< 0.008 (0.00203)	0.013 ± 0.005 (0.00203)	0.023 ± 0.012 (0.00203)	0.014 ± 0.007 (0.00203)	< 0.012 (0.00203)	< 0.015 (0.000734)
5037.4	< 0.008 (0.00507)	$\frac{3}{2}^-$	0.045 ± 0.010 (0.00507)	< 0.008 (0.00111)	< 0.008 (0.00112)	< 0.010 (0.000810)	< 0.010 (0.000810)	< 0.012 (0.000810)	< 0.012 (0.000830)	< 0.015 (0.000734)
5019.4	0.006 ± 0.004 (0.00101)	$\frac{3}{2}^-$	< 0.005 (0.00101)	< 0.008 (0.00101)	< 0.008 (0.00101)	< 0.010 (0.00101)	< 0.010 (0.00101)	< 0.012 (0.00101)	< 0.012 (0.00101)	< 0.015 (0.00344)

resonances.

5311 (613;  $l=2; \frac{5}{2}^+$ ). The  $\frac{5}{2}^+$  assignment is probable, as this state is not seen in any of the  $\frac{1}{2}^+$  resonances.

5293\* (631 keV;  $l=2; \frac{3}{2}^+$ ). A  $\gamma$  ray at this energy is visible in the 401-, 2175.8-, 2460-, 2610-, 3260-, 4013-, 4567-, and the 4844-eV  $p$ -wave resonances and in the 2546- and 4475-eV  $s$ -wave resonances. The probable spin-parity assignment is  $\frac{3}{2}^+$ . The line is well established in the present work, but has not been seen in previous experiments.

5133 (792;  $l=2; \frac{3}{2}^+$ ). This line shows up in the 612- ( $\frac{1}{2}^-$ ) and 2176-eV ( $\frac{1}{2}^-$ ) resonance spectra, ruling out a  $\frac{5}{2}^+$  assignment.

5037 (887;  $l=2; \frac{3}{2}^+$ ). Populated by  $s$ -wave resonances at 1525 and 2546 eV, this level must have a  $\frac{3}{2}^+$  assignment. We identify this level with  $l=2$ , level seen at 896 keV in ( $d, p$ ).

5019 (905;  $l=0; \frac{1}{2}^+$ ). This level was not resolved in the ( $d, p$ ) experiment.

The levels below were not included in the valence

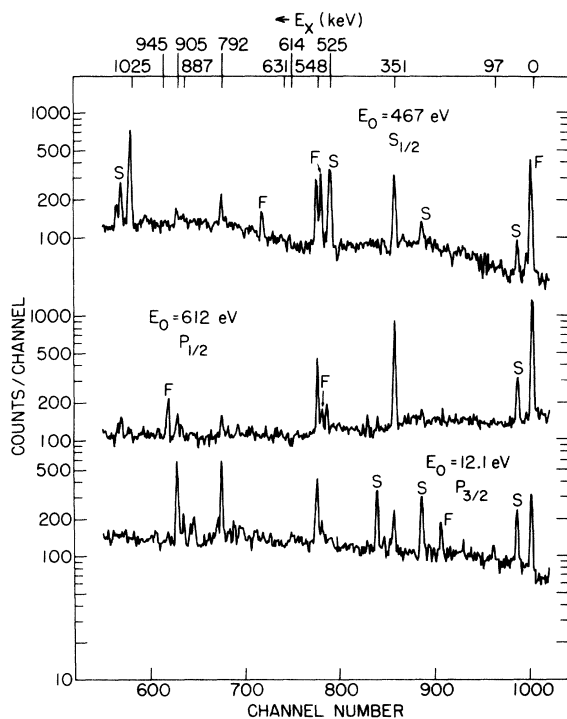


FIG. 3. Portions of the pulse height spectra for three resonances. The 467-eV resonance is an  $s$ -wave resonance. The 12 eV is a  $p$ -wave resonance of modest strength. The 612-eV resonance is a very strong  $p$ -wave resonance showing good correlation to the valence model. The peaks labeled S and F are single escape and full energy peaks, while the unlabeled major peaks are two-escape peaks corresponding to transition to excited states shown on the energy scale.

analysis because of lack of ( $d, p$ ) spectroscopic data.

4979.4 (945; ?; ?). Seen in 817-, 1122-, and 1919-eV  $\frac{3}{2}^-$  resonances.

4899.6 (1024;  $l=1; \frac{1}{2}^-, \frac{3}{2}^-$ ). This negative parity state is seen in the spectra of the 467- and 2546-eV  $\frac{1}{2}^+$  resonances. We identify this state with that at 1033 keV in the ( $d, p$ ) work.

4758.2\* (1166;  $l=?; \frac{1}{2}^-, \frac{3}{2}^-, \frac{5}{2}^+$ ). Very strongly fed level in 817-eV resonance, also fed in 401 eV. Strength demands a positive parity state here, previously unreported.

4670.7 (1253;  $l=?; \frac{1}{2}^-, \frac{3}{2}^-, \frac{5}{2}^+$ ). This level is fed in several  $\frac{3}{2}^-$  resonances. This might be identified with the 1261-keV level reported in ( $d, p$ ).

4542.6 (1382;  $l=2?; \frac{3}{2}^+, \frac{5}{2}^+$ ). Fed in five  $\frac{3}{2}^-$  resonances; may be identifiable with the 1391-keV  $l=2$  level seen in  $d, p$ .

4469 (1455; ?; ?). This level is weakly populated in both  $s$ - and  $p$ -wave resonances. We cannot definitely establish its parity.

4391.4\* (1533; ?; ?). Seen in both  $s$ - and  $p$ -wave resonances, so parity cannot be definitely established.

4365.4 (1559; ?; ?). This line is fed in both  $s$ - and  $p$ -wave resonances, and may be identified with the 1558-keV level seen in ( $d, t$ ).

4353.5\* (1571; ?; ?). This level is not seen elsewhere, but is fed in both  $s$ - and  $p$ -wave resonances.

4289.7 (1635; ?; +). Strongly fed in 12-, 401-, 817-, and 2943-eV  $p$ -wave resonances, and is probably positive parity.

4263 (1661; ?; ?). This level is fed in both  $s$ - and  $p$ -wave resonances. It may be identifiable with the 1672-keV level seen in ( $d, p$ ).

4214 (1710;  $l=1; \frac{1}{2}^-, \frac{3}{2}^-$ ). We feed this level in both  $s$ - and  $p$ -wave resonances. The energy is close to a level seen in radioactivity (1707), and may be identified with the  $l=1$  level seen in ( $d, p$ ) at 1722 keV.

4183 (1741;  $l=2; \frac{3}{2}^+, \frac{5}{2}^+$ ). This level is probably spin  $\frac{3}{2}$ , as it is populated from the 467-eV  $\frac{1}{2}^+$  resonance. We identify it with the  $l=2$  level seen in ( $d, p$ ) at 1755 keV.

4037\* (1887; ?; ?). This line is seen primarily in the 12-eV resonance. It has not been reported elsewhere.

3996 (1928; ?; ?). Strongly populated in  $s$  resonances and therefore probably *negative* parity. May be identifiable with the 1920 keV ( $p, d$ ) or the 1920 keV ( $d, t$ ) level, but probably not with the 1930-keV ( $d, p$ ) level with  $l=0$ .

3975\* (1950; ?; ?). Populated from both  $s$ - and  $p$ -wave resonances. May be identifiable with  $l=0$  ( $d, p$ ) levels at 1965 keV.

3869\* (2055; ?; +). Strongly populated in  $p$ -wave resonances.

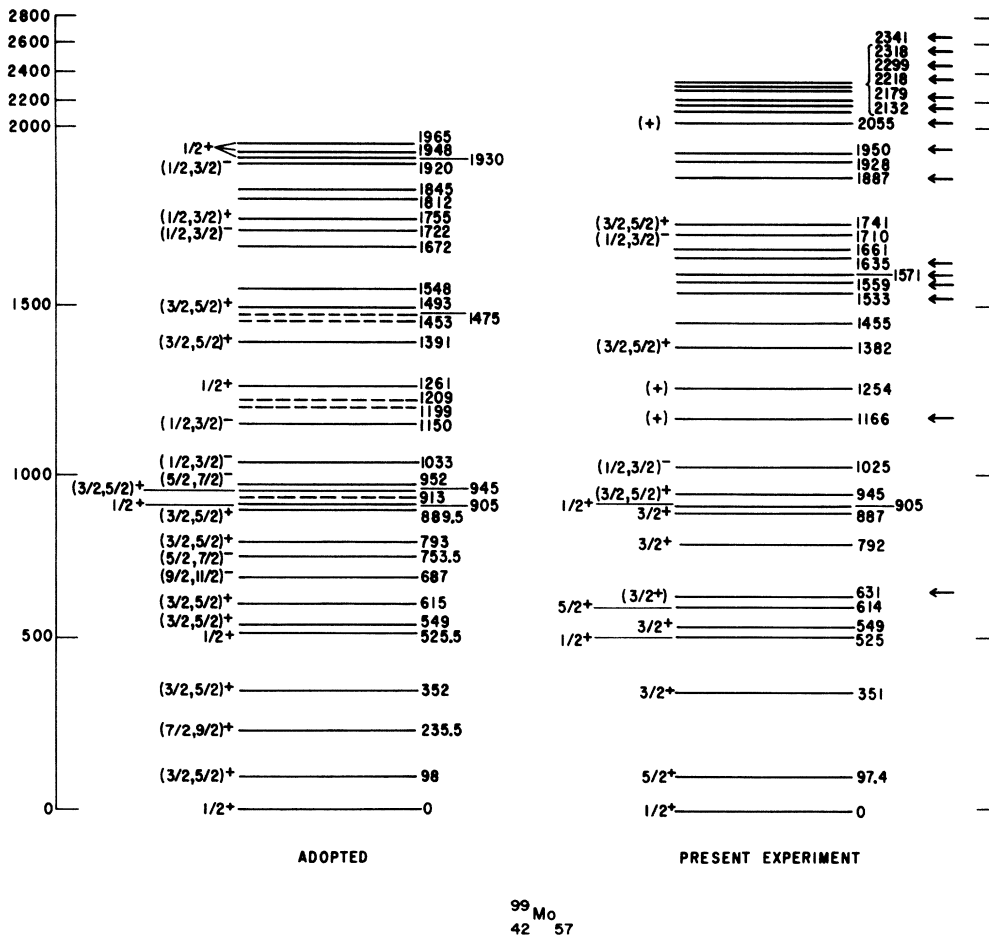


FIG. 4. Level scheme for  ${}^{99}\text{Mo}$  from the present experiment. The levels populated by  $(n, \gamma)$  transitions from the capturing state are shown compared with previously adopted levels in  ${}^{99}\text{Mo}$  (Ref. 32). The arrows highlight new levels.

Other  $\gamma$  rays which appear in both  $s$ - and  $p$ -wave resonances, and for which no evidence exists from other experiments are the following: 3792, 3745, 3706, 3625, 3606, and 3584.

B. Neutron resonance parameters of  ${}^{98}\text{Mo}$

Figures 5 and 6 show, respectively, the cumulative reduced neutron width summation for iden-

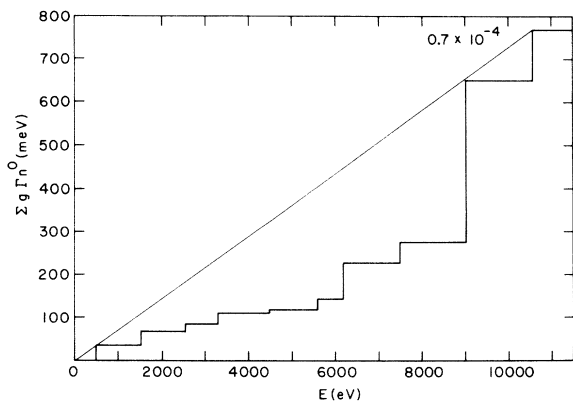


FIG. 5. Cumulative plot of  $g\Gamma_n^0$  versus energy for  $s$ -wave resonances in  ${}^{98}\text{Mo}$ .

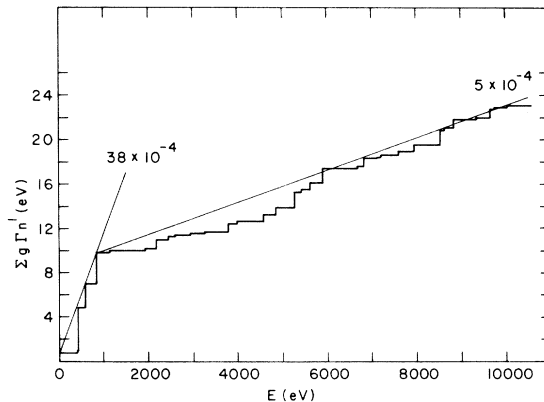


FIG. 6. Cumulative plot of  $g\Gamma_n^1$  versus energy for  $p$ -wave resonances in  ${}^{98}\text{Mo}$ .

tified *s*- and *p*-wave resonances in  $^{98}\text{Mo}$ . The striking step in the case of the *p*-wave resonances is immediately obvious and relevant to the discussion of valence transitions. In the region of the step—below 1 keV—the local strength function is  $\sim 38 \times 10^{-4}$ , as compared with a global average of  $7 \times 10^{-4}$ . The resonances responsible for this remarkable fluctuation—the 429-, 612-, and 817-eV resonances, have reduced widths of larger than  $10^{-3}$  of a single particle width. We, therefore, expect that single particle effects in the radiative decay of the resonances will be emphasized in this region.

Parity assignments for the neutron resonances were made as discussed in Sec. II A. Spin assignments for *p*-wave resonances below 5300 eV were either taken from previous work<sup>25</sup> or assigned on the basis of the  $\gamma$ -ray spectra. In the latter case the  $\frac{5}{2}^-$  levels at 97 and at 613 keV were especially useful, since transitions consistent with *E*1 strengths to those levels allowed fixing resonance spins at  $\frac{3}{2}^-$ . All the  $\frac{3}{2}^-$  members of the set of 17 resonances showed measurable strengths to the  $\frac{5}{2}^+$  final states except for the 3794- and 2610-eV resonances. None of the  $\frac{1}{2}^-$  resonances showed a measurable population of these  $\frac{5}{2}^+$  states, as expected. Thus there were no inconsistencies between our experiment and the previously reported spin assignments for these *p*-wave resonances.

The previous resonance parameters listed in Ref. 25 were derived primarily from the work of Weigmann, Rohr, and Winter,<sup>29</sup> Shwé and Coté,<sup>27</sup> Wynchank, Garg, Havens, and Rainwater,<sup>24</sup> and Pevzner *et al.*<sup>30</sup> and unpublished work of Newstead.<sup>26</sup> Weigmann's work involved capture cross section measurements, from which neutron widths can be derived only indirectly, by assuming values for the total radiation width. As we shall see, the single particle contributions can cause considerable variations in  $\Gamma_\gamma$  from resonance to resonance. The work of Shwé *et al.* and Wynchank *et al.* involved natural molybdenum samples, and thus the extraction of  $^{98}\text{Mo}$  widths is complicated by the presence of other isotopes. None of the previous work extends past 10 keV. For these reasons we believe the present set of resonance parameters to be considerably more accurate than previous results. The sensitivity of the present experiment is such that we do not expect to have missed a significant number of levels below 10 keV. The sensitivity ranges from 0.1 eV at 10 keV to 0.7 eV at 20 keV, and 2.2 eV at 50 keV for the smallest detected neutron width.

#### IV. DISCUSSION OF VALENCE MODEL

To the results of Tables III–VII, we address first the following basic question: Are the radia-

tive widths and neutron widths in this sample statistically independent of one another? A quantitative way to formulate this question is to investigate the relationship between widths through the linear correlation coefficient  $\rho$ . From the theoretical considerations of Lane and Lynn, we know that for direct reaction mechanisms which bypass compound nucleus formation, the radiative width amplitude will be proportional to the product of the initial and final state reduced widths, namely,

$$\Gamma_{\gamma\lambda f}^{1/2} \propto \theta_\lambda \theta_f,$$

where  $\lambda$  refers to resonance state,  $f$  refers to the final state of the residual nucleus,  $\theta_\lambda^2 \equiv \gamma_\lambda^2 / \gamma_{sp}^2$ ,  $\gamma_\lambda^2 \equiv \Gamma_\lambda / 2P$ ,  $\gamma^2$  are reduced widths,  $\gamma_{sp}^2$  are reduced widths for single particle transitions, and  $P$  are penetrabilities.

Several closely related models have been proposed for direct reaction ( $n, \gamma$ ) effects in resonances. The simplest is the channel capture of Lane and Lynn,<sup>1,2</sup> which assigns the single particle effects to configuration space outside the nuclear radius. By considering just the external contributions from the bound final and free initial states they obtain from a first order perturbation theory calculation:

$$\Gamma_{\gamma\lambda f}(\text{ch}) = \frac{16\pi}{9} k_\gamma^3 \left(\frac{2}{R}\right) \theta_f^2 \theta_i^2 \left(\frac{\bar{e}R}{k_f}\right)^2 \times \frac{|\langle j'IJ_\lambda || Y^1 || j''Ij \rangle|^2}{2J_\lambda + 1}.$$

By including the interior portion of the wave functions, as calculated from an optical model code, Lynn<sup>4</sup> has modified this expression and obtained what is known as the valence model prediction:

$$\Gamma_{\gamma\lambda f}(\text{sp}) = \frac{16\pi}{9} k^3 \theta_\lambda^2 \theta_f^2 \left| \bar{e} \int_0^\infty dr u_\lambda r u_f \right|^2 \times \frac{|\langle j'IJ_\lambda || Y^1 || j''Ij \rangle|^2}{2J_\lambda + 1},$$

where  $\bar{e} \equiv eZ/A$ , the effective neutron charge, and  $k = 2\pi E_\gamma / \hbar c$ . Note that by comparison of these two models, they become identical if we set

$$\left| \int_0^\infty dr u_\lambda r u_f \right|^2 = \left(\frac{2}{k_f}\right)^2,$$

$$\text{where } k_f = (2ME_\gamma / \hbar)^{1/2}.$$

Detailed calculations show, in fact, that for reasonable optical model parameters the overlap integral has values in the range 0.1 to 0.2 b, which is quite comparable to  $(2/k_f)^2$  for states bound by  $\sim 5$  to 6 MeV. Thus to within a factor of

TABLE VIII. Valence model parameters and overlap integrals.

Transition	Radius (fm)	$I^2$ Overlap integral (b)	$\frac{4\pi \langle j'IJ_\lambda  Y^1  j''IJ\rangle ^2}{2J_\lambda+1}$
		$V_0 = 42.8 \text{ MeV}$	
		$V_{so} = 9.875 \text{ MeV}$	
		$a = 0.69 \text{ fm}$	
		$W = 0 \text{ (bound states)}$	
		$V = \frac{-V_0}{1 + \exp(r-R)/a}$	
		$-V_{so} \left(\frac{\hbar}{m_\pi c}\right)^2 \frac{1}{r} \frac{d}{dr} V  \vec{1} \cdot \vec{\sigma} $	
$3p_{1/2} \rightarrow 3s_{1/2}$	6.369	0.206	1
$3p_{1/2} \rightarrow 2d_{3/2}$	6.369	0.104	2
$3p_{3/2} \rightarrow 3s_{1/2}$	6.1704	0.221	1
$3p_{3/2} \rightarrow 2d_{3/2}$	6.1704	0.114	1/5
$3p_{3/2} \rightarrow 2d_{5/2}$	6.1704	0.099	9/5
$\gamma_{sp}^2(3p_{1/2}) = 0.144 \text{ MeV (evaluated at 12 fm)}$			
$\gamma_{sp}^2(3p_{3/2}) = 0.124 \text{ MeV (evaluated at 12 fm)}$			

$\sim 2$ , the simple channel capture model approximates the results of the more detailed valence model.

A detailed valence model calculation was carried out for  $^{98}\text{Mo}$  neutron capture using the optical model code ABACUS-2 with a Woods-Saxon potential.<sup>40</sup> The required overlap integrals were calculated by adjusting the potential parameters to produce single particle  $3p_{1/2}$  and  $3p_{3/2}$  near the neutron threshold (actually 1 keV below threshold), and integrals for  $p_{1/2, 3/2} \rightarrow s_{1/2}$  and  $p_{1/2, 3/2} \rightarrow d_{3/2, 5/2}$  were obtained. As has been pointed out previously by Vogt,<sup>41</sup> the diffuse edge of the Woods-Saxon potential causes difficulties in defining the neutron penetrability, since hard sphere penetrabilities are conventionally used in converting experimentally observed widths to reduced widths. Vogt has suggested multiplying the single particle width for  $s$  waves by a factor  $(1 + 6.7a^2)$ , where  $a$  is the diffuseness parameter. Vogt does not give expressions for  $p$ -wave capture. We have avoided such difficulties by choosing a larger radius, which is far beyond the potential range. At this radius, hard-sphere penetrabilities are still valid, and the effects of potential diffuseness are thus avoided. The use of the larger radius does not, of course, affect the observable widths; it merely redefines the factorization of the width into a penetrability and reduced width. In accordance with the definition of reduced width, the wave function normalization is referred to this arbitrary radius, which we have chosen as 12 fm. This procedure results in reduced widths considerably smaller than those conventionally obtained.

The parameters and results of the detailed calculations are summarized below in Table VIII. Also listed there are the values for the angular part of the reduced matrix elements. The values

of Table VIII do not, in fact, differ by more than about 20% from the calculations of Lynn,<sup>4</sup> which used initial states bound by 100 keV, used a wave function normalization over all space, and evaluated the integrals for  $A \approx 120$ .

With these overlap integrals, we calculated the predicted widths of the model for the 17  $p$ -wave resonances of the present experiment. To obtain widths we used penetrabilities evaluated at 12 fm, as described above

$$\theta_\lambda^2 = \frac{\Gamma_{n\lambda}/2P(12 \text{ fm})}{\gamma_{sp}^2(12 \text{ fm})},$$

and  $\theta_\lambda^2$  were obtained from the  $(d, p)$  experiments of Moorhead and Moyer.<sup>36</sup> The widths are tabulated in Table IX. To obtain intensities which can be compared with experiment, two additional steps must be done:

(a) Correction for angular correlations to yield intensities at  $90^\circ$ . These correction factors are 1.25, 0.8, and 1.05 for  $3/2 \rightarrow 1/2$ ,  $3/2 \rightarrow 3/2$ , and  $3/2 \rightarrow 5/2$ , respectively.

(b) Correction for total radiative widths. The assumption that single particle effects are important implies a significant variation in total radiative width  $\Gamma_\gamma$ , from resonance to resonance, depending on the neutron width. Since these  $\Gamma_\gamma$  are largely unknown, or poorly measured, we adopted the following procedure. We summed the valence contributions from the 10 final states for each of the 17 resonances. When the valence contribution was subtracted from the measured total radiation widths (where known) the average, 90 meV, was found to be very close to the 86-meV average for  $s$ -wave resonances, for which no significant valence component is expected. We therefore assumed that 88 meV is a good estimate for the statistical contribution to the total radiative width.

TABLE IX. Partial widths calculated from the valence model. All table entries in eV, except where noted &lt; less than 0.0001.

$E_\gamma$ (keV)	$J^\pi$	$S$	$E_0$ (eV)								
			12.1 $\frac{3}{2}$	401 $\frac{3}{2}$	428.8 $\frac{1}{2}$	611.8 $\frac{1}{2}$	817.3 $\frac{3}{2}$	1121.9 $\frac{3}{2}$	1919.5 $\frac{3}{2}$	2175.8 $\frac{1}{2}$	
			$\Gamma_n^1$ (eV)								
			0.375	0.0895	3.99	2.10	1.40	0.12	0.0375	0.81	
5924.4	$\frac{1}{2}^+$	0.67	0.0075	0.0018	0.0641	0.0337	0.0281	0.0024	0.0008	0.0130	
5827.0	$\frac{5}{2}^0$	0.21	0.0018	0.0005	...	...	0.0067	0.0005	0.0002	...	
5573.1	$\frac{3}{2}^0$	0.11	0.0001	<	0.0089	0.0047	0.0004	<	<	0.0002	
5399.8	$\frac{1}{2}^0$	0.042	0.0004	0.0001	0.0030	0.0016	0.0014	0.0001	<	0.0006	
5375.8	$\frac{3}{2}^0$	0.43	0.0004	0.0001	0.0312	0.0164	0.0014	0.0001	<	0.0063	
5310.6	$\frac{5}{2}^0$	0.018	0.0001	<	...	...	0.0005	<	<	...	
5293.1	$\frac{3}{2}^0$	0.0	<	<	<	<	<	<	<	<	
5132.6	$\frac{3}{2}^0$	0.0425	<	<	0.0027	0.0014	0.0001	<	<	0.0005	
5037.4	$\frac{3}{2}^0$	0.0925	0.0001	<	0.0055	0.0029	0.0002	<	<	0.0011	
5019.4	$\frac{1}{2}^0$	0.021	0.0001	<	0.0012	0.0006	0.0005	<	<	0.0002	
Valence component sum (meV)			10.5	2.5	116.6	61.3	39.3	3.1	1.0	21.9	
$\Gamma_\gamma = 88 + \Gamma_\gamma$ (valence)			98.5	90.5	204.6	149.3	127.3	91.1	89.0	109.9	
$\langle \Gamma_\gamma \rangle$ s wave = 86 meV											
$\langle \Gamma_p \rangle - \Gamma_\gamma$ valence = 90 meV											
$E_\gamma$ (keV)	$J^\pi$	$S$	$E_0$ (eV)								
			2460 $\frac{1}{2}$	2610 $\frac{3}{2}$	2943 $\frac{1}{2}$	3260 $\frac{1}{2}$	3794 $\frac{3}{2}$	4013 $\frac{3}{2}$	4567 $\frac{5}{2}$	4844 $\frac{3}{2}$	5268 $\frac{5}{2}$
			$\Gamma_n^1$ (eV)								
			0.37	0.05	0.072	0.053	0.387	0.165	0.26	0.298	0.745
5924.4	$\frac{1}{2}^+$	0.67	0.0059	0.0010	0.0011	0.0008	0.0078	0.0034	0.0052	0.0060	0.0149
5827.0	$\frac{5}{2}^0$	0.21	...	0.0002	...	...	0.0018	0.0008	0.0013	0.0014	0.0036
5573.1	$\frac{3}{2}^0$	0.11	0.0008	<	0.0002	0.0001	0.0001	<	<	0.0001	0.0002
5399.8	$\frac{1}{2}^0$	0.042	0.0003	<	0.0001	<	0.0004	0.0002	0.0002	0.0003	0.0007
5375.8	$\frac{3}{2}^0$	0.43	0.0029	<	0.0006	0.0004	0.0004	0.0002	0.0002	0.0003	0.0008
5310.6	$\frac{5}{2}^0$	0.018	...	<	...	...	0.0001	<	0.0001	0.0001	0.0003
5293.1	$\frac{3}{2}^0$	0.0	<	<	<	<	<	<	<	<	<
5132.6	$\frac{3}{2}^0$	0.0425	0.0002	<	<	<	<	<	<	<	0.0001
5037.4	$\frac{3}{2}^0$	0.0925	0.0005	<	0.0001	0.0001	0.0001	<	<	0.0001	0.0001
5019.4	$\frac{1}{2}^0$	0.021	0.0001	<	<	<	0.0001	0.0001	0.0001	0.0001	0.0003
Valence component sum			10.7	1.2	2.1	1.4	10.8	4.7	7.1	8.4	21.0
$\Gamma_\gamma = 88 + \Gamma_\gamma$ (valence)			98.7	89.2	90.1	89.4	98.8	92.7	95.1	96.4	109.0

TABLE X. Overall correlations and significance levels for  $^{98}\text{Mo}$  transitions.

Transitions	Number of cases	$r$	$P$
All E1 allowed	158	+0.70	>0.999
$s_{1/2}$ final states	51	+0.78	>0.999
$d_{3/2}$ final states	85	+0.55	>0.999
$d_{5/2}$ final states	22	+0.15	0.745

The photon intensities were then computed from  $I_{\gamma\lambda f}(\text{valence}) = \Gamma_{\gamma\lambda f}(\text{valence}) / [0.088 + \sum_f \Gamma_{\gamma\lambda f}(\text{valence})]$ . This procedure is more consistent than using some average value for  $\Gamma_{\gamma}$ , and avoids the large errors introduced by directly using measured values for  $\Gamma_{\gamma}$  for each resonance. The intensities so computed are shown in Table VII, in parentheses below the corresponding experimental numbers.

In the idealized case of only direct reactions, the correlation  $\rho$  between the widths  $\Gamma_{\gamma\lambda f}$  and  $\theta_{\lambda}^2 \theta_f^2$  would be unity. However, it is quite clear that statistical processes account for some fraction of the resonance widths; indeed, for most nuclides in the medium to heavy mass region the statistical contribution is the major one, in agreement with the Bohr hypothesis of independence of formation and decay of the compound nucleus. We therefore write an expression for  $\Gamma_{\gamma\lambda f}$  which explicitly includes a statistical component in addition to the single particle amplitude  $A(\text{sp})$ :

$$\Gamma_{\gamma\lambda f} = |A_{\gamma\lambda f}(\text{sp}) + A_{\gamma\lambda f}(\text{CN})|^2,$$

where the statistical amplitude  $A_{\gamma\lambda f}(\text{CN})$  displays no correlation with initial and final state width amplitudes. In this case the width correlation coefficient  $\rho = \text{corr}\{\Gamma_{\gamma\lambda f}, \theta_{\lambda}^2 \theta_f^2\}$  will be reduced by an amount  $\langle \Gamma_{\gamma\lambda f}(\text{sp}) \rangle / \langle \Gamma_{\gamma\lambda f}(\text{sp}) \rangle + \langle \Gamma_{\gamma\lambda f}(\text{CN}) \rangle$ .

The measured width correlation  $\rho$  thus directly gives the average single particle fraction of the average radiative width  $\langle \Gamma_{\gamma\lambda f} \rangle \equiv \langle \Gamma_{\gamma\lambda f}(\text{sp}) \rangle + \langle \Gamma_{\gamma\lambda f}(\text{CN}) \rangle$ , as has been shown previously by Beer.<sup>7</sup>

## V. DISCUSSION OF RESULTS

The comparison of model with experimental results suggests strongly that the valence model accounts for a considerable part of the reaction mechanism in neutron capture in  $^{98}\text{Mo}$ ; for the resonances in particular at 429 and 612 eV, where  $\theta^2 = \gamma^2 / \gamma^2(\text{sp})$  is approximately  $10^{-3}$ , about  $\frac{1}{2}$  the strength is carried by valence transitions.

A correlation analysis is useful here in quantitatively establishing that we are seeing a real dependence of radiative strength on single particle widths, and not some statistical quirk. Let us denote the linear correlation coefficient for a finite sample size by  $r$  and the corresponding coefficient for the parent population by  $\rho$ . If we examine the linear correlation coefficient between the model prediction and the experimental result, for our limited sample size,

$$r = \text{corr}\{I_{\gamma\lambda f}(\text{valence}), I_{\gamma\lambda f}(\text{measured})\},$$

then we are in essence examining the correlation between our measured values and the product  $\theta_{\lambda}^2 \theta_f^2$ . Such a correlation calculation has been carried out for the set of 17 resonances and 10 final states. We have further subdivided the transitions according to specific final states and specific resonances.

The probability  $P$  in Table X is that for obtaining a sample correlation coefficient  $r$  lower than the observed  $r$ , when the limited sample is drawn from a population of independent random variables,

TABLE XI. Correlations with neutron widths.

$E_{\gamma}$ (keV)	Intercept <sup>a</sup>	Slope <sup>a</sup>	$r$ (correlation)	$\Delta_r$ <sup>b</sup>	$P$ (significance)
5924.4	-0.03	0.87	+0.76	0.03	>0.999
5827.05			+0.055	...	0.53
5573.1	+0.004	3.4	+0.98	0.04	>0.999
5399.8			-0.08	...	0.42
5375.8	+0.004	0.514	+0.87	0.06	0.998
5310.6			-0.25		c
5293.1	...	...	...	...	... <sup>c</sup>
5132.6			-0.24		0.23
5037.4			-0.24		0.36
5019.4			-0.003		0.50

<sup>a</sup> Intercept and slope calculated from a least-squares regression analysis of  $y = mx + b$ , where  $y$ 's are observed and  $x$ 's calculated intensities, for cases where  $r$  is significant.

<sup>b</sup>  $\Delta_r$  calculated where significance is in excess of 0.95 before correction for experimental errors;  $(r - 2\Delta r)$  is then retested for significance.

<sup>c</sup> Insufficient sample size to establish significance level.

TABLE XII. Correlations with final state spectroscopic factors.

Resonance energy	$b^a$	$m^a$	$r$	$\Delta r^b$	$P$
12.1			+0.05		0.55
401			+0.31		0.80
428.8	-0.002	0.845	+0.86	0.04	>0.999
611.8	-0.003	1.04	+0.86	0.03	>0.999
817.3	-0.002	0.40	+0.95	0.03	>0.999
1121.9			+0.22		0.73
1919.5			-0.38		0.14
2175.8			+0.31		0.80
2460			+0.23		0.73
2610			+0.12		0.63
2943			+0.75	0.24	0.75
3260			+0.66	0.21	0.75
3794	-0.001	0.942	+0.96	0.12	0.99
4013			+0.06		0.56
4567	-0.0003	2.46	+0.73	0.09	0.95
4844			+0.58	0.28	0.52
5268			-0.03		0.47

<sup>a</sup>Intercept and slope calculate from a least-squares regression analysis of  $y = mx + b$ , where  $y$ 's are observed and  $x$ 's calculated intensities, for cases where  $r$  is significant.

<sup>b</sup>See previous table.

i.e.  $\rho$ , the population correlation coefficient, is zero. The conclusion is therefore that the above correlations are highly significant, except for the  $p_{3/2} - d_{5/2}$  transitions, for which no effect can be established.

The significance level has been calculated using Fisher's transformation,<sup>42</sup>  $z = \frac{1}{2} \ln[(1+r)/(1-r)]$ , which reduces the  $r$  distribution to near-Gaussian form. We have made detailed checks on the validity of Fisher's transformation by Monte Carlo techniques. Populations with normal, Porter-Thomas, and random distributions were employed. We are convinced, on the basis of these tests, that Fisher's transformation is not significantly worse than a Monte Carlo calculation down to a sample size  $n = 5$ . Hence we have used Fisher's transformation in this work. We have also calculated correlations  $r$  for (a) the model prediction for each resonance and (b) for each final state. These correlations are calculated in Tables XI and XII, and are given with the appropriate significance level. For some of these sets, the statistical errors in the measured intensities are as important as the effects of finite sample size. The effect of the statistical error is included by calculating, after Clement,<sup>43</sup>

$$\Delta_r^2 \equiv \sigma_r^2 = \frac{\sum_i \epsilon_i^2 (b_i - \bar{b})^2}{\sum_i (b_i - \bar{b})^2 (a_i - \bar{a})^2},$$

where  $\epsilon_i$  is the error in  $a_i$ . For those cases where the subtraction of  $2\sigma_r = 2\Delta r$  to the observed value  $r$  does not decrease  $P$  below 0.95, we assume that we have definitely established a correlation.

An examination of these tables indicates that correlations with  $\theta_\lambda^2$  can be definitely established only for transitions to the  $\frac{1}{2}^+$  ground state (5924 keV), the  $\frac{3}{2}^+$  351-keV state (5573 keV), and the  $\frac{3}{2}^+$  548-keV state (5376). Note that the correlations result almost completely from the  $\frac{1}{2}^+$  resonances

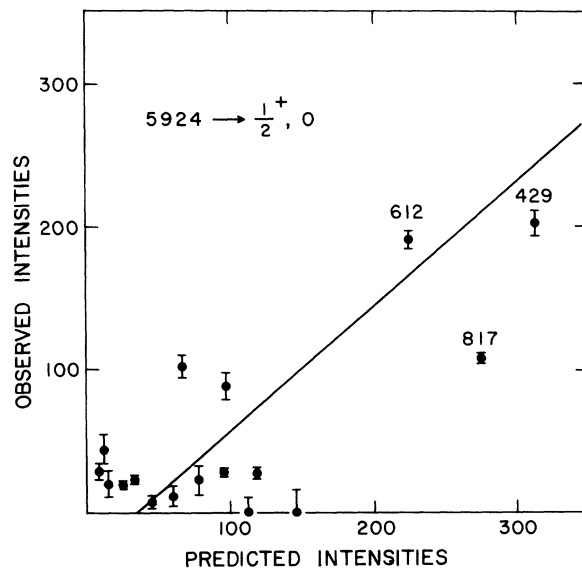


FIG. 7. A comparison of predicted vs measured radiative widths for the ground state transition. The straight line is a least-squares regression fit to  $y = mx + b$ , where  $y$  is the prediction of the valence model, and  $x$  the observed intensities. The intensities are given in photons per 1000 captures.

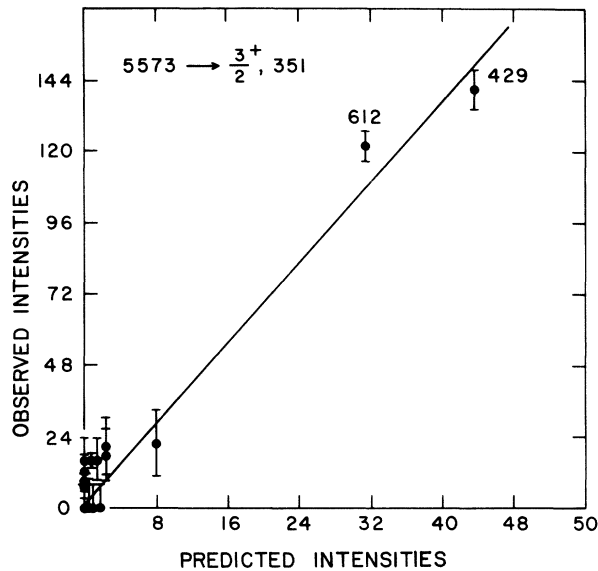


FIG. 8. Predicted versus measured intensities to the  $\frac{3}{2}^+$  351-keV state of  $^{99}\text{Mo}$ .

at 429 and 612 eV. Removal of these would remove the correlation.

In the case of the ground state transition, the model, on average predicts the size of the transitions reasonably well, as well as accounting for the correlations. This is shown clearly from the results of the linear regression analysis given in Table XI.

For the 5573-keV transitions, the observed values are much larger than the valence prediction, while for the 5376-keV transitions the opposite is true. Thus for these highly correlated transitions, the valence model is unable to make quantitative predictions. This fact cannot be attributed to the presence of statistical components masking the direct mechanism, as should be evident from Figs. 7-9. It is clear from these figures that the contribution of the 612- and 429-eV resonances is much larger than statistical fluctuations would permit. Even for the relatively weaker 5573- and 5376-keV transitions, the observed strengths in the 612- and 429-eV resonances are many times larger than statistically expected; hence, a direct comparison to the valence model is valid. The fact that the model both *underpredicts* and *overpredicts* the transition strength shows that a scale factor change, such as a change in effective charge, for example, would not improve agreement.

Correlations with  $\theta_p^2$  can be definitely established for the  $\frac{1}{2}^-$  429-eV, the  $\frac{1}{2}^-$  612-eV, the  $\frac{3}{2}^-$  817-eV, the  $\frac{3}{2}^-$  3794-eV, and possibly ( $P=0.95$ ) the  $\frac{3}{2}^-$  4567-eV resonances. The finite sample

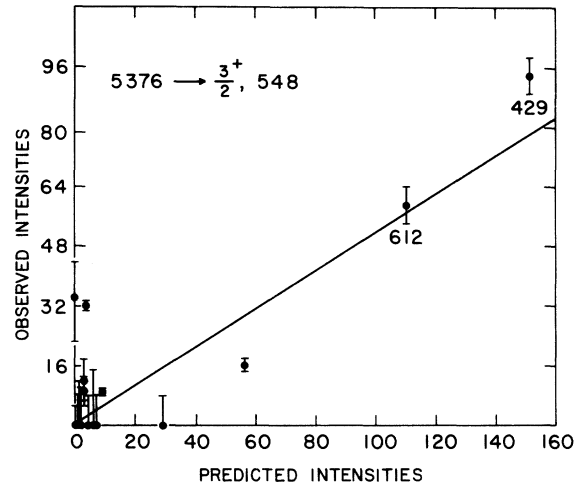


FIG. 9. Predicted versus measured intensities to the  $\frac{3}{2}^+$  548-keV state of  $^{99}\text{Mo}$ .

size, and limited statistics, prevent us from making definite statements about the other resonances. The 429, 612, and 817 are the resonances with the largest reduced widths and can therefore be expected to show these correlations. We note, however, that the valence model considerably overpredicts the intensities for the 817-eV resonance. These three resonances have dimensionless reduced widths of the order of  $10^{-3}$  single particle units.

In summary, the valence model provides a qualitative description of the transitions from  $p_{1/2}$  resonances to the  $s_{1/2}$  ground state, predicting a correlation with the reduced widths of the initial and final states and giving the right order of magnitude for the intensities for the very strong resonances. The model does not work quantitatively for transitions to the  $\frac{3}{2}^+$  and  $\frac{5}{2}^+$  excited states from  $\frac{3}{2}^-$  resonances. For the  $\frac{5}{2}^+$  final states, no correlation has been established from our data. For the  $\frac{3}{2}^+$  final states, the correlations observed are not adequately explained by the model because the predicted magnitudes of the intensities do not agree with observed intensities. For these cases we must postulate an alternative reaction mechanism, possibly involving doorway states of the type predicted by Beer,<sup>7</sup> Beres, and Soloviev.<sup>9</sup> The presence of these doorway states are also suggested by the structure seen in the  $p$ -wave strength function. Similar conclusions have been suggested by Wasson and Slaughter<sup>17</sup> for the case of capture in  $^{92}\text{Mo}$ . We have at present, however, no quantitative way to calculate these intensities from available models. It is hoped that these models can be developed in the near future.

We wish to acknowledge the valuable assistance of Roger Byrd, Jean Domish, and Susanna Solovey with the preparation of our results. We have also had helpful discussions and advice from E. H.

Auerbach, O. A. Wasson, S. F. Mughabghab, M. R. Bhat, and Karim Rimawi. The authors wish to thank H. I. Liou for a valuable discussion of the application of Bayes' theorem.

\*Work supported by the U. S. Energy Research and Development Administration.

†Permanent address: Periphonics Corporation, Bohemia, New York 11716.

<sup>1</sup>A. M. Lane, Nucl. Phys. **11**, 625 (1959).

<sup>2</sup>A. M. Lane and J. E. Lynn, Nucl. Phys. **11**, 646 (1959); **17**, 586 (1960).

<sup>3</sup>A. M. Lane and R. G. Thomas, Rev. Mod. Phys. **30**, 257 (1958).

<sup>4</sup>J. E. Lynn, *The Theory of Neutron Resonance Reactions* (Clarendon, Oxford, 1968), p. 330.

<sup>5</sup>C. F. Clement, A. M. Lane, and J. R. Rook, Nucl. Phys. **66**, 273, 293 (1965); see also G. Brown, *ibid.* **57**, 339 (1964).

<sup>6</sup>M. Potokar, Phys. Lett. **46B**, 530 (1973).

<sup>7</sup>M. Beer, Ann. Phys. (N.Y.) **65**, 181 (1971).

<sup>8</sup>G. A. Bartholomew, E. D. Earle, A. J. Ferguson, J. W. Knowles, and M. A. Lone, *Advances in Nuclear Physics* (Plenum, New York, 1973), Vol. 7, p. 229.

<sup>9</sup>V. G. Soloviev and V. V. Voronov, JINR Dubna Report No. 1975 E4 8834 (unpublished) [*Yad. Phys.* (to be published)]; W. P. Beres and M. Divadeenam, Phys. Rev. Lett. **25**, 596 (1970); W. P. Beres (private communication).

<sup>10</sup>J. Kopecky, A. M. J. Spits, and A. M. Lane, Phys. Lett. **B49**, 323 (1974).

<sup>11</sup>S. F. Mughabghab, R. E. Chrien, O. A. Wasson, G. W. Cole, and M. R. Bhat, Phys. Rev. Lett. **26**, 1118 (1971).

<sup>12</sup>M. A. Lone, R. E. Chrien, O. A. Wasson, M. R. Bhat, and H. R. Muether, Phys. Rev. **174**, 1512 (1968).

<sup>13</sup>A. M. Lane, in *Proceedings of the Second International Symposium on Neutron Capture  $\gamma$ -Ray Spectroscopy and Related Topics*, Petten, 1971 (Reactor Centrum Nederland, Petten, 1975).

<sup>14</sup>L. M. Bollinger, in *Proceedings of the International Conference on Photoneuclear Reactions and Applications*, Asilomar, 1973, edited by B. L. Berman (Lawrence Livermore Laboratory, Livermore, 1973), p. 783.

<sup>15</sup>R. E. Chrien, *Radiative Decay of Neutron-Resonant States, Nuclear Structure Study with Neutrons* (Plenum, London, 1974), p. 101.

<sup>16</sup>F. Becvar, in *Proceedings of the Second International School of Neutron Physics (Alushta, Dubna, 1974)* (Joint Institute of Nuclear Research, Dubna, 1974), p. 294.

<sup>17</sup>O. A. Wasson and G. G. Slaughter, Phys. Rev. C **8**, 297 (1973).

<sup>18</sup>R. E. Toohy and H. E. Jackson, Phys. Rev. C **9**, 346 (1974).

<sup>19</sup>K. Rimawi and R. E. Chrien (see Ref. 13).

<sup>20</sup>K. Rimawi and R. E. Chrien (see Ref. 13).

<sup>21</sup>R. E. Chrien, *Statistical Properties of Nuclei* (Plenum, New York, 1972), p. 233.

<sup>22</sup>S. E. Atta and J. A. Harvey, ORNL Report No. 3205 (unpublished).

<sup>23</sup>E. Migneco, J. P. Theobald, and S. DeJonge, Lett. Nuovo Cimento **4**, 1220 (1970).

<sup>24</sup>S. Wynchank, J. B. Garg, W. W. Havens, Jr., and J. Rainwater, Phys. Rev. **166**, 1234 (1967).

<sup>25</sup>*Resonance Parameters*, compiled by S. F. Mughabghab and D. I. Garber, Brookhaven National Laboratory Report No. BNL-325 (National Technical Information Service, Springfield, Virginia, 1973), 3rd. ed., Vol. I.

<sup>26</sup>C. Newstead, AERE Report No. AERE-PR/NP-10, 8, 1967 (unpublished).

<sup>27</sup>H. Shwé and R. E. Coté, Phys. Rev. **179**, 1148 (1969).

<sup>28</sup>L. M. Bollinger and G. E. Thomas, Phys. Rev. **171**, 1293 (1968).

<sup>29</sup>H. Weigmann, G. Rohr, and J. Winter, in *Proceedings of the Third Conference on Neutron Cross Sections and Technology* (Conf-710301, National Technical Information Center, Springfield, Virginia, 1971), Vol. 2, p. 749.

<sup>30</sup>M. I. Pevzner, Yu. V. Adamchuk, L. S. Danelyan, B. V. Efimov, S. S. Moskalev, and G. V. Muradyan, Zh. Eksp. Teor. Fiz. **44**, 1187 (1963) [*Sov. Phys.—JETP* **17**, 1187 (1963)].

<sup>31</sup>A. H. Wapstra and N. B. Gove, Nucl. Data **9**(Nos. 4, 5) (1971), The 1971 Atomic Mass Evaluation.

<sup>32</sup>W. R. Kane (unpublished).

<sup>33</sup>G. D. Loper, G. E. Thomas, and L. M. Bollinger, Nucl. Instrum. Methods **121**, 581 (1974).

<sup>34</sup>G. A. Bartholomew, Annu. Rev. Nucl. Sci. **11**, 259 (1961).

<sup>35</sup>P. Cavallini, J. Blachot, E. Monnard, and A. Moussa, Radiochem. Acta. **15**, 105 (1971).

<sup>36</sup>J. B. Moorhead and R. A. Moyer, Phys. Rev. **184**, 1205 (1969).

<sup>37</sup>R. C. Diehl, B. L. Cohen, R. A. Moyer, and L. H. Goldman, Phys. Rev. C **1**, 2132 (1970).

<sup>38</sup>T. Ishimatsu, S. Hayashiki, N. Kawamura, T. Awaya, H. Ohmura, Y. Nakajima, and S. Mitarai, Nucl. Phys. **A185**, 273 (1972).

<sup>39</sup>L. R. Medsker, Nucl. Data Sheets **12**, 431 (1974).

<sup>40</sup>E. H. Auerbach, BNL Report No. 6562, Nov. 1962 (unpublished), revised August 1964.

<sup>41</sup>E. Vogt, Rev. Mod. Phys. **34**, 723 (1962).

<sup>42</sup>M. G. Kendall and Alan Stuart, *The Advanced Theory of Statistics* (Hafner, New York, 1969).

<sup>43</sup>A. M. Lane, Ann. Phys. (N.Y.) **63**, 171 (1971).